Demonstration of a Narrow Energy Spread, ~0.5 GeV Electron Beam from a Two-Stage Laser Wakefield Accelerator

B. B. Pollock,[1,2,*] C. E. Clayton,[3] J. E. Ralph,[1] F. Albert,[1] A. Davidson,[3] L. Divol,[1] C. Filip,[1] S. H. Glenzer,[1] K. Herpoldt,[4] W. Lu,[5,3] K. A. Marsh,[3] J. Meinecke,[1] W. B. Mori,[3] A. Pak,[3] T. C. Rensink,[1] J. S. Ross,[1] J. Shaw,[3] G. R. Tynan,[2] C. Joshi,[3] and D. H. Froula[1,†]

[1]*Lawrence Livermore National Laboratory, 7000 East Avenue, Livermore, California 94550, USA*
[2]*University of California, San Diego, 9500 Gilman Drive, La Jolla, California 92093, USA*
[3]*University of California, Los Angeles, 405 Hilgard Avenue, Los Angeles, California 90095, USA*
[4]*University of Oxford, Wellington Square, Oxford, OX1 2JD, United Kingdom*
[5]*Department of Engineering Physics, Tsinghua University, Beijing, China, 100084*

(Received 13 April 2011; published 18 July 2011)

Laser wakefield acceleration of electrons holds great promise for producing ultracompact stages of GeV scale, high-quality electron beams for applications such as x-ray free electron lasers and high-energy colliders. Ultrahigh intensity laser pulses can be self-guided by relativistic plasma waves (the wake) over tens of vacuum diffraction lengths, to give >1 GeV energy in centimeter-scale low density plasmas using ionization-induced injection to inject charge into the wake even at low densities. By restricting electron injection to a distinct short region, the injector stage, energetic electron beams (of the order of 100 MeV) with a relatively large energy spread are generated. Some of these electrons are then further accelerated by a second, longer accelerator stage, which increases their energy to ~0.5 GeV while reducing the relative energy spread to <5% FWHM.

DOI: 10.1103/PhysRevLett.107.045001 PACS numbers: 52.38.Kd, 41.75.Jv, 52.35.Mw

State-of-the-art conventional radio-frequency linear accelerators currently produce electron beams with up to 50 GeV energies by staging many 100 MeV sections [1]. Future proposed x-ray free electron lasers (such as the European XFEL) will produce 20 GeV electron beams which, when passed through an undulator, will provide extremely bright x-ray sources. Facilities of this scale require substantial lengths (several kilometers) to achieve high electron energies due to limits on the maximum accelerating gradient imposed by cavity damage threshold considerations (< 100 MeV/m). Alternatively, laser wakefield accelerators (LWFAs) can support gradients exceeding 100 GeV/m [2,3], opening the possibility of dramatically reducing the required length to produce high-energy beams. Current laser technology limits the length of these devices to a few centimeters and, therefore, the energy gain to a few GeV. Coupling of multiple independent high-energy gain LWFA stages could provide a path forward for achieving future compact, high-energy particle sources.

Recent experiments have demonstrated self-guiding [4] of ultrashort laser pulses in the blowout regime of a LWFA, where extremely nonlinear wakefields are produced in underdense plasmas [5–12]. In this regime the rising edge of an intense, short laser pulse tunnel ionizes low-Z gas, and the ponderomotive force of the laser expels electrons radially outward to a maximum distance $R \simeq 2\sqrt{a_0}c/\omega_p$ [13], determined by balancing the transverse ponderomotive force with the restoring space charge force of the stationary ions. Here $a_0 = eA/mc$ is the normalized vector potential of the laser, and $\omega_p = \sqrt{n_e e^2/\epsilon_0 m_e}$ is the electron plasma frequency. The blown-out region at the front of the pulse acts as a channel to guide the majority of the laser light, while behind the laser pulse electrons are pulled back toward the axis. This produces an electron plasma wave (the wake) with a phase velocity v_ϕ nearly equal to the group velocity v_g of the laser.

When the laser pulse length approaches $c\tau \approx R$, a nearly spherically shaped wake is formed, within which nearly all of the electrons are blown out. The trajectories of these electrons form a sheath around the ions [14], and the longitudinal electric field structure near the axis of the wake is ideal for accelerating a high-quality electron beam [15]. Electrons injected into the wake (via self-injection [16], ionization-induced injection [17–19], colliding pulses [20], etc.) become trapped in the wake potential if they gain a longitudinal velocity $v = v_\phi$ and continue accelerating in the longitudinal electric field of the wake (of the order of 100 GeV/m for electron densities of $\sim 10^{18}$ cm^{-3} [13]). Over a dephasing length $L_{\mathrm{deph}} \simeq (2/3)(\omega_{\mathrm{Laser}}^2/\omega_p^2)R$, these electrons, traveling at nearly c, move forward in the wake to its midplane, where the sign of the electric field reverses and electrons decelerate. The dephasing limited energy gain is given by $W_{\max} = E_z L_{\mathrm{deph}} = 0.37(P[\mathrm{TW}])^{1/3}(n_e/10^{18}\ \mathrm{cm}^{-3})^{-2/3}$, where E_z is the dephasing length averaged electric field within the wake [13]. Therefore, for powers less than 80 TW, electron densities below 2×10^{18} cm^{-3} are required to achieve electron energy gains above 1 GeV in this regime.

At such low electron densities, it becomes difficult to self-trap electrons in the wake with fully ionized low-Z gases (He, H_2) [5,11,21–24] because the wake potential cannot be driven to large enough amplitude with presently available laser systems (~100 TW) [18,21]. Adding a small concentration of high-Z dopant gas with a large step in ionization potential for the two K-shell electrons to the low-Z background gas provides a new source of trapped electrons—ionization-induced injection [18]—at densities approaching 1×10^{18} cm^{-3} and has allowed for ~1.5 GeV energy gain in centimeter-scale plasmas [6]. The inherent drawback to both self- and ionization-induced injection is that charge is continuously injected into the wake, leading to a large energy spread in the accelerated beam.

In this Letter, we report that, by limiting ionization-induced injection to a distinct region, a 460 MeV electron beam with <5% energy spread is produced. The experiments are performed with an 8 mm long, two-stage gas cell, shown schematically in Fig. 1. The cell is comprised of a 3 mm injection stage, filled with a mixture of 99.5% He and 0.5% N_2 gas, separated by a 1 mm diameter aperture from an immediately adjacent 5 mm acceleration stage containing pure He. This result is obtained at an electron density where self-trapping in He is not observed, and spectroscopic measurements of the gas species along the cell indicate that the N_2 is confined to the injector stage. The spatial and spectral content of the laser beam at the exit of the gas cell imply that the laser is both self-guided and drives a wake over the entire length of the injector and accelerator stages.

These studies were conducted at the Jupiter Laser Facility, Lawrence Livermore National Laboratory, with the Callisto laser system. The laser beam, which delivers up to 200 TW of power in a 60 fs laser pulse, is focused with an $f/8$, off-axis parabolic mirror to a vacuum spot size w_0 of 15 μm at the $1/e^2$ intensity point (containing 30% of the laser power) at a position 750 μm inside the gas cell. For coupled laser powers of 30–60 TW $a_0 =$ 2–2.8, while the ionization thresholds to produce N^{6+} and N^{7+} are 1.8 and 2.3, respectively. Therefore, K-shell electrons from the nitrogen gas in the injector stage will be continuously ionized near the peak of the laser pulse, which resides near the zero crossing of the longitudinal electric field. This injection phase is near-optimum for trapping because these electrons can now experience the entire potential difference within the wake [18].

Figure 2(a) shows electron beam data on the first of two image plates from injector-only and injector + accelerator experiments. The electrons are dispersed by the dipole magnet and are recorded on two image plates to determine independently their energy and exit angle upon leaving the plasma [1,25]. The corresponding spectra are shown in

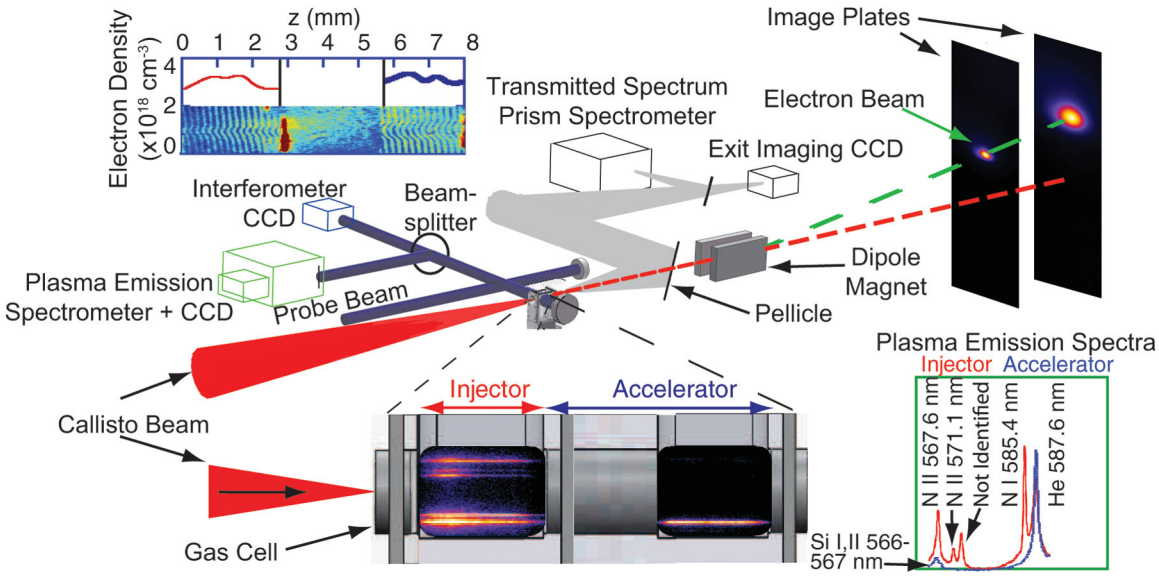

FIG. 1 (color). Schematic of the experimental setup showing the 800 nm Callisto laser beam (in red), the two-stage gas cell, the 800 nm probe beam (in blue), a measured interferogram with its associated Abel inverted density profile (above the interferometer CCD camera), the plasma emission spectrometer and CCD camera, plasma emission images (shown inside the gas cell windows) with the spatially resolved plasma emission spectrum along the laser axis from each stage of the gas cell, the vacuum laser axis after the gas cell (red dashed line), the 0.42 T dipole magnet (20 cm long, centered 66 cm from the exit of the gas cell), the deflected electron trajectory (green dashed line) onto the image plates (located 132 and 192 cm from the exit of the gas cell), and the optical path of the transmitted laser light (in gray) to an imaging system and a prism spectrometer. The transverse size of the plasma observed in the interferogram is larger in the accelerator section because the noncoupled (and therefore unguided) diffracting laser light ionizes a volume larger than the sub-50 μm wake, which is not resolved by this diagnostic. Optical access for the transverse diagnostics is provided by constructing the walls of the gas cell from microscope slides pressed against rubber gaskets to form a seal. The source of the Si line in the plasma emission image is suspected to be minute amounts of Si outgassing from the gaskets under vacuum. The gas cell entrance (exit) aperture is 0.5 (2.0) mm.

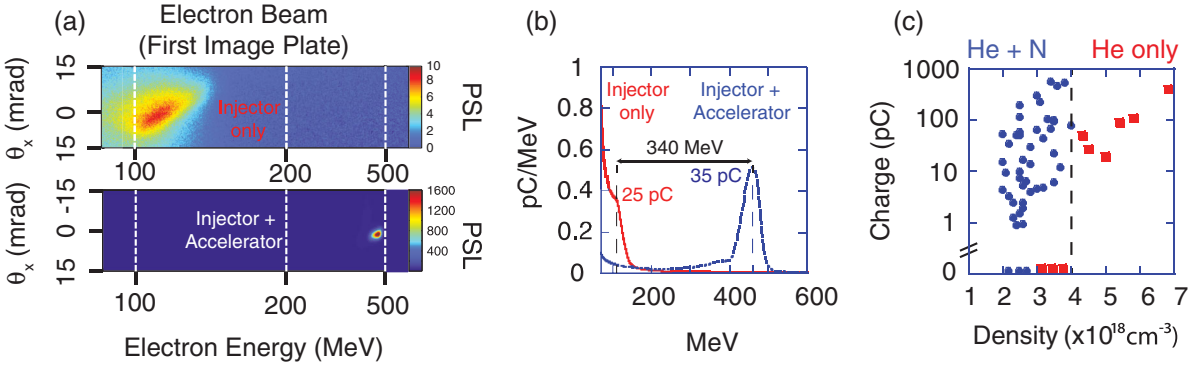

FIG. 2 (color). (a) Magnetically dispersed electron beam images from a 4 mm injector-only gas cell (top) and the 8 mm two-stage cell (bottom). (b) Electron spectra above 70 MeV for the 8 mm two-stage injector-accelerator cell (blue curve) filled to an electron density of 3×10^{18} cm^{-3} in each stage for a coupled laser power of 40 TW and the 4 mm injector-only cell (red curve) filled to an electron density of 3.4×10^{18} cm^{-3} for a coupled laser power of 50 TW. The injector gas fill in each case is 99.5% He and 0.5% N_2, and the total charge is indicated for each spectrum. (c) The total observed charge above 70 MeV for injector gas fills of pure He (red squares) and 99.5% He with 0.5% N_2 (blue circles) for coupled laser powers between 30 and 60 TW.

Fig. 2(b), where a 460 ± 25 MeV electron beam containing $\sim$35 pC of charge is produced in the two-stage cell with a density of $3 \pm 0.3 \times 10^{18}$ cm^{-3} (see Fig. 1; the standard deviation of the longitudinal density profile is 5.6%) for a coupled laser power of 40 TW. The injector-only spectrum is broad, consistent with ionization-induced injection [18], and exhibits a slight peak at 120 MeV. Conversely, after deconvolution in quadrature of the 2.3 mrad transverse beam size with the spectrum of Fig. 2(b), the energy spread ΔE of the two-stage experiment is inferred to be 5%.

A Mach-Zehnder interferometer allows the electron density to be measured along the gas cell with a spatial resolution of 125 μm and is timed such that the 100 fs probe beam traverses the plasma $\sim$20 ps after the main beam has exited the gas cell. While injector-only data were taken for densities as low as 2×10^{18} cm^{-3}, the minimum density where the injector and accelerator densities were matched was 3×10^{18} cm^{-3}. Because of the additional electrons from the fully ionized nitrogen atoms in the injector, the neutral gas pressure in the accelerator must be slightly higher than in the injector in order to balance the electron density between the two stages. This results in a small upstream pressure, which helps to confine the nitrogen to the injector. The gas species in each stage is determined by 1:1 imaging the plasma emission along the laser propagation axis onto the 50 μm entrance slit of a 1/3-m spectrometer coupled to a 16-bit charge-coupled device (CCD) camera, where the spectral resolution of the system is 2.5 Å. As illustrated by the plasma emission lines in Fig. 1, which correspond to the same experiment shown in the interferogram, nitrogen is present in the injector stage only. As shown in Fig. 2(c), no self-injected electrons are observed in pure He plasma for electron densities below 4×10^{18} cm^{-3} (at coupled laser powers $\leq$ 60 TW). This, along with the absence of nitrogen lines in the accelerator stage, indicates that the observed electrons are from the nitrogen dopant gas in the injector.

Figure 3 shows the spatial and spectral transmitted laser light properties for the injector-only and the two-stage gas cell, which demonstrate self-guiding and wakefield excitation in the self-guided blowout regime. Most of the transmitted light is confined to 100–130 μm FWHM spots, which are much smaller than the unguided, vacuum spot sizes at those planes, and indicates the laser pulse was self-guided in both cases. Figures 3(c) and 3(d) show the respective ''open-slit'' spectra of the transmitted light, where the spectral features are dominated by the guided, bright features of Figs. 3(a) and 3(b). The spectrum corresponding to the injector-only case shows the expected blue- and redshifts arising from photon acceleration or ionization [26] and local pump depletion [27], respectively, experienced by portions of the incident laser pulse as it produces the plasma and excites the wake within the injector stage. In the longer, two-stage case, the extent of the redshifting approximately doubles compared with the injector-only data, indicating that, in addition to the laser pulse continuing to self-guide across the interface between the two stages, the wake is also driven over the extended distance.

Three-dimensional particle-in-cell simulations performed with the massively parallel code OSIRIS [28]—utilizing a moving window and an Ammosov-Delone-Krainov [29] ionization model—demonstrate the essential features of this injector-accelerator concept. The simulations were initialized with the nominal experimental parameters, where the 40 TW laser beam was focused to a Gaussian diffraction limited spot size of 15 microns at the top of a plasma density ramp followed by a uniform 8 mm long (3 mm He/N_2 gas, 5 mm He only) 3.0×10^{18} cm^{-3} plasma. These simulations used a 130 μm $\times$ 180 μm $\times$ 180 μm computational window corresponding to $4000 \times 300 \times 300$ grid points.

The simulation tracks the 6D phase space of the He, N L-shell and N K-shell electrons. In the injector portion of the simulation, the trapping is mainly of the N K-shell

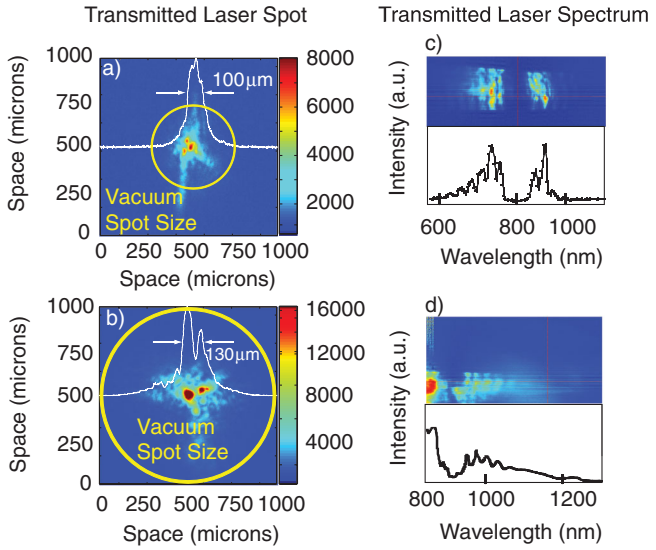

FIG. 3 (color). (a),(b) Images of the transmitted laser light at the exit of the 4 mm injector stage and the 8 mm two-stage gas cell, respectively. Vertically integrated lineouts indicate the guided laser spot size, while the vacuum laser spot size at the exit of the cell is denoted for each case by a yellow circle. A long-pass filter is placed in front of the camera to attenuate unshifted and blueshifted light. (c),(d) The transmitted laser spectrum from the injector-only and the two-stage cell, respectively. A mask is used to block the fundamental 800 nm light to take better advantage of the dynamic range of the 8-bit, frame-grabbed, infrared camera. The spectral fringes are due to the etalon effect of the uncoated pellicle beam splitter (5 μm thick at 45°) seen in Fig. 1. For each spectrum, the recorded false-color image is shown.

electrons, which were ionized close to the peak of the laser pulse. Although some He electrons are trapped towards the end of the accelerator section, the final energy spectrum is predominantly comprised of the N K-shell electrons that form a 510 MeV peak with a ± 20 MeV energy spread. Both beam loading and phase space dynamics of the electrons are important in narrowing the eventual energy spread, and the details of this simulation will be published elsewhere. As has been reported previously [5,6], the injected charge in the present simulation is significantly greater than what is observed in the experiments presented here. This is likely a result of the nonideal initial laser conditions present in the experiment (e.g., pulse front tilt [30], non-Gaussian laser spot).

In conclusion, a centimeter-scale, two-stage injector-accelerator LWFA is shown to generate ~ 0.5 GeV electron beams with $<5\%$ energy spread containing 35 pC of charge by using the ionization-induced injection mechanism. Extending the present work to densities approaching 1×10^{17} cm^{-3} could provide a compact platform for producing high-quality, 10 GeV electron beams with petawatt-class lasers for advanced light source and collider applications [31].

We thank R. Cauble, D. Price, S. Maricle, and J. Bonlie for their support of the Callisto laser system. This work was performed under the auspices of the Department of Energy by the Lawrence Livermore National Laboratory, the University of California at San Diego, and the University of California at Los Angeles under Contracts No. DE-AC52-07NA27344, No. DE-FG03-92ER40727, No. DE-FG02-92ER40727, No. DE-FC02-07ER41500, and No. DE-FG52- 09NA29552 and NSF Grants No. PHY-0936266 and No. PHY-0904039. This work was partially funded by the Laboratory Directed Research and Development Program under project tracking code 08-LW-070.

*pollock6@llnl.gov
†Present address: Laboratory for Laser Energetics, 250 E. River Road, Rochester, NY 14623, USA.

[1] I. Blumenfeld *et al.*, Nature (London) **445**, 741 (2007).
[2] T. Tajima and J. M. Dawson, Phys. Rev. Lett. **43**, 267 (1979).
[3] E. Esarey *et al.*, Rev. Mod. Phys. **81**, 1229 (2009).
[4] J. E. Ralph *et al.*, Phys. Rev. Lett. **102**, 175003 (2009).
[5] D. H. Froula *et al.*, Phys. Rev. Lett. **103**, 215006 (2009).
[6] C. E. Clayton *et al.*, Phys. Rev. Lett. **105**, 105003 (2010).
[7] A. G. R. Thomas *et al.*, Phys. Rev. Lett. **98**, 095004 (2007).
[8] J. Faure *et al.*, Nature (London) **431**, 541 (2004).
[9] C. G. R. Geddes *et al.*, Nature (London) **431**, 538 (2004).
[10] S. P. D. Mangles *et al.*, Nature (London) **431**, 535 (2004).
[11] N. A. M. Hafz *et al.*, Nat. Photon. **2**, 571 (2008).
[12] A. Maksimchuk *et al.*, Phys. Plasmas **15**, 056703 (2008).
[13] W. Lu *et al.*, Phys. Rev. ST Accel. Beams **10**, 061301 (2007).
[14] W. Lu *et al.*, Phys. Rev. Lett. **96**, 165002 (2006).
[15] J. B. Rosenzweig *et al.*, Phys. Rev. A **44**, R6189 (1991).
[16] F. S. Tsung *et al.*, Phys. Rev. Lett. **93**, 185002 (2004).
[17] E. Oz *et al.*, Phys. Rev. Lett. **98**, 084801 (2007).
[18] A. Pak *et al.*, Phys. Rev. Lett. **104**, 025003 (2010).
[19] C. McGuffey *et al.*, Phys. Rev. Lett. **104**, 025004 (2010).
[20] J. Faure *et al.*, Nature (London) **444**, 737 (2006).
[21] J. E. Ralph *et al.*, Phys. Plasmas **17**, 056709 (2010).
[22] T. Matsuoka *et al.*, in *Proceedings of the Thirteenth Advanced Accelerator Concepts Workshop, Santa Cruz, CA, 2008* (AIP, New York, 2009), pp. 184–189.
[23] S. Kneip *et al.*, Phys. Rev. Lett. **103**, 035002 (2009).
[24] P. Dong *et al.*, Phys. Rev. Lett. **104**, 134801 (2010).
[25] B. B. Pollock *et al.*, in *Proceedings of the 2009 Particle Accelerator Conference, Vancouver, 2009* (http://epaper.kek.jp/PAC2009/papers/we6rfp101.pdf), p. A14.
[26] C. W. Siders *et al.*, Phys. Rev. Lett. **76**, 3570 (1996).
[27] C. D. Decker *et al.*, Phys. Plasmas **3**, 2047 (1996).
[28] R. Fonseca *et al.*, Lect. Notes Comput. Sci. **2331**, 342 (2002).
[29] M. V. Ammosov *et al.*, Sov. Phys. JETP **64**, 1191 (1986).
[30] A. Popp *et al.*, Phys. Rev. Lett. **105**, 215001 (2010).
[31] S. F. Martins *et al.*, Nature Phys. **6**, 311 (2010).